J. Electrochem. Sci. Eng. **16** (2026) 3278; https://doi.org/10.5599/jese.3278

Open Access : : ISSN 1847-9286
https://pub.iapchem.org/ojs/index.php/JESE

Original scientific paper

Electrochemical deposition of thin bifunctional Co-P films and investigation of their electrocatalytic and corrosion properties in the hydrogen evolution reaction and oxygen evolution reaction

Aygun Oruj Zeynalova[1], Akif Shikhan Aliyev[1], Ruhangiz Gurmuz Guseynova[1], Ulviyya Magsud Gurbanova[1,✉], Natavan Sharafaddin Soltanova[1], Samir Bahram Safarov[1], Shafag Shamsaddin Bayramova[2], Telli Islam Hamzayeva[2] and Dunya Mahammad Babanly[3]

[1]*Institute of Chemistry PLE, Ministry of Science and Education of the Republic of Azerbaijan, H. Javid 113, 1143, Baku, Azerbaijan*
[2]*Institute of Geology PLE, Ministry of Science and Education of the Republic of Azerbaijan, Baku, Azerbaijan*
[3]*French-Azerbaijani University, Azerbaijan State Oil and Industry University, Nizami str. 183, Baku, Azerbaijan*

Corresponding Authors: ✉mailto:*uqurbanova92@gmail.com*; Tel: +994702756030

Received: March 4, 2026; Accepted: June 18, 2026; Published: June 30, 2026

Abstract

At present, the rapid growth of the global economy, together with the accelerated depletion of fossil fuel resources, has led to growing concerns about the availability and sustainability of energy. Therefore, renewable energy sources such as solar, hydrogen, and wind energy are of critical importance. Compared with other hydrogen production methods, water electrolysis offers several advantages, including sustainability, low cost, high efficiency, and the absence of harmful atmospheric emissions. In recent decades, water electrolysis as a hydrogen production technology has been extensively investigated. The development of new, efficient, and cost-effective electrocatalysts for water electrolysis remains a crucial challenge. Cobalt-phosphorus thin films are promising candidates for replacing expensive noble-metal-based electrocatalysts. In the present work, bifunctional Co-P thin films were synthesized via a one-step electrodeposition method from an acidic electrolyte. The as-deposited films were amorphous; however, after annealing, two orthorhombic phases, Co_2P and CoP, were identified by X-ray diffraction analysis. The prepared films were characterized using X-ray phase analysis, scanning electron microscopy, and energy-dispersive X-ray spectroscopy. The electrocatalytic properties of the coatings were investigated before and after annealing in both neutral (0.5 M Na_2SO_4) and alkaline (1 M KOH) media for the hydrogen and oxygen evolution reactions. In addition, the corrosion behaviour of the Co-P thin films was examined, and it was established that the amorphous, non-annealed films exhibited superior corrosion resistance in alkaline media.

Keywords
Transition metal phosphide, electrochemical codeposition; thin coating films; water electrolysis; electrocatalysis; corrosion resistance

Introduction

The rapid development of the global economy has led to the rapid depletion of fossil fuel resources, raising concerns about the types and amounts of energy consumed and their significant impact on the climate [1-3]. Hydrogen production *via* water splitting using solar energy is one of the most attractive pathways for generating renewable fuels. The development of active and stable catalysts composed of earth-abundant elements for hydrogen and oxygen evolution is a key requirement for the successful production of green fuels.

For renewable energy sources such as solar and wind power, advanced energy storage systems with high power and high energy density are essential [4-6]. Elements from the iron subgroup demonstrate superior performance in water electrolysis for hydrogen production, particularly in neutral and alkaline media, where they offer an optimal balance of cost, stability, and catalytic activity [7,8].

Recently, considerable attention has been given to transition-metal phosphides and phosphates, which have successfully replaced their oxide and hydroxide counterparts in supercapacitors. Transition metal phosphides, such as nickel and cobalt phosphides (Co_2P, Ni_2P), are attractive candidates due to their abundance, low cost, and high electrochemical activity [9-12]. These phosphides exhibit excellent redox activity, desirable electrical conductivity, and high theoretical energy capacity [13]. They are widely available in nature and environmentally friendly [14-16].

Among these, cobalt phosphides are particularly notable for their outstanding electrocatalytic performance and stability in the hydrogen evolution reaction (HER) across all pH values, as well as their favourable properties when used as anode materials in lithium-ion batteries [17-20]. Metal phosphides are typically synthesized *via* phosphidation of metallic or oxide nanoparticles [21], through solid-state reactions using precursor salts [22], or by electrodeposition [23,24]. Transition metal phosphides obtained electrochemically are often bifunctional and have been used in water electrolysis as both cathodes and anodes [25-27].

Metal phosphides can be synthesized from several different phosphorus sources. For example, when an inorganic phosphate such as NaH_2PO_2 is used, hypophosphite can react with metal ions under neutral or mildly acidic conditions to form the corresponding metal phosphide [24]. Cobalt phosphide (Co-P) has attracted significant attention from researchers as an efficient bifunctional electrocatalyst based on non-noble metals [28].

Electrodeposited Co-P films with very low phosphorus content but excellent activity for both hydrogen evolution reaction (HER) and oxygen evolution reaction (OER) were obtained by J.Nan *et al.* [23]. Electrocatalytic activity tests were performed in 1 M KOH solution. Elemental analysis of the films confirmed a uniform distribution of Co and P throughout the film after HER.

Cobalt phosphide (Co-P) nanospheres were developed as non-noble metal electrocatalysts via a one-step electrodeposition method [29]. The morphology of the Co-P nanostructures and their electrocatalytic activity in HER were controlled by the applied potentials during electrodeposition. Linear sweep voltammetry demonstrated that Co-P grown at -0.9 V exhibited the best performance for HER.

In this work, the electrochemical deposition of bifunctional Co-P thin films from an acidic aqueous electrolyte is investigated. The obtained films exhibit electrocatalytic activity in both neutral and alkaline media, along with satisfactory corrosion resistance under alkaline conditions.

Experimental

The co-deposition of cobalt with phosphorus was investigated by recording cyclic and linear polarization curves, including chronoamperometry and chronopotentiometry, using an IVIUMSTAT Electrochemical Interface potentiostat. These measurements were conducted in a three-electrode cell equipped with a jacket to maintain a constant electrolyte temperature. The electrolyte temperature was maintained using a UTU-4 universal ultra thermostat. A platinum electrode with a geometric surface area of 0.4 cm^2 served as the working electrode, while a platinum plate with a geometric surface area of 4 cm^2 was used as the counter electrode. A silver/silver chloride electrode (Ag/AgCl) in a saturated KCl solution served as the reference electrode, and all potentials are reported with respect to this reference.

To determine elemental composition, morphology, electrocatalytic, and corrosion properties, Co-P thin films were electrodeposited onto a copper electrode with a geometric surface area of 2 cm^2 in a two-electrode cell under galvanostatic conditions. The electrolyte was prepared by dissolving the following components in distilled water: 0.1 M $CoSO_4$, 0.12 M NaH_2PO_4, 0.5 M H_3BO_3, 0.14 M Na_2SO_4 and 0.001 M $NaC_{12}H_{25}SO_4$. The pH of the solution was adjusted to 3.6. All reagents were purchased from Sigma-Aldrich (Germany). Electrodeposition was carried out at a current density of 10 mA cm^{-2} over a temperature range of 50 °C K for 4 hours. Prior to deposition, the surface of the copper electrode was etched in an HNO_3 : H_2O (1 : 1) solution, followed by rinsing with ethanol and acetone. A platinum plate was used as the anode.

The as-deposited films exhibited an amorphous structure and were thermally treated in air at 450 °C for 1 hour. The morphology and elemental composition of the films were examined using a JEOL (Japan) scanning electron microscope (SEM) equipped with an energy-dispersive X-ray (EDX) spectrometer from Oxford Instruments. Phase analysis was performed using a Rigaku Miniflex-500 X-ray diffractometer with CuKα radiation (λ = 0.154 nm).

The electrocatalytic properties of the films were evaluated by recording cathodic and anodic polarization curves in both neutral (0.5M Na_2SO_4) and alkaline (1M KOH) media, followed by the construction of Tafel plots. Corrosion behaviour was studied in an alkaline medium using chronopotentiometry.

Results and discussion

Figure 1 shows the overall cyclic polarization curve for the co-deposition of cobalt with phosphorus, realized by potential changes starting from 1.0 V *vs*. Ag/AgCl to lower potential values. In the cathodic branch of the polarization curve, it can be seen that the co-deposition of these two elements occurs within the potential range of -0.5 to -0.9 V. At potentials more negative than -0.9 V, hydrogen evolution begins. On the anodic branch, an anodic dissolution peak of the deposited film appears at a potential of -0.2 V.

The deposition proceeds according to Equation (1) [29,30].

$$Co^{2+} + H_2PO_2^- + 2H^+ + 3e^- \rightarrow CoP + 2H_2O \quad (1)$$

Cobalt cations (Co^{2+}) and hypophosphite anions ($H_2PO_2^-$) in solution are reduced to their corresponding atomic forms, Equations (2) and (3) [31,32].

$$Co^{2+} + 2e^- \rightarrow Co \quad (2)$$

$$H_2PO_2^- + 2H^+ + e^- \rightarrow P + 2H_2O \quad (3)$$

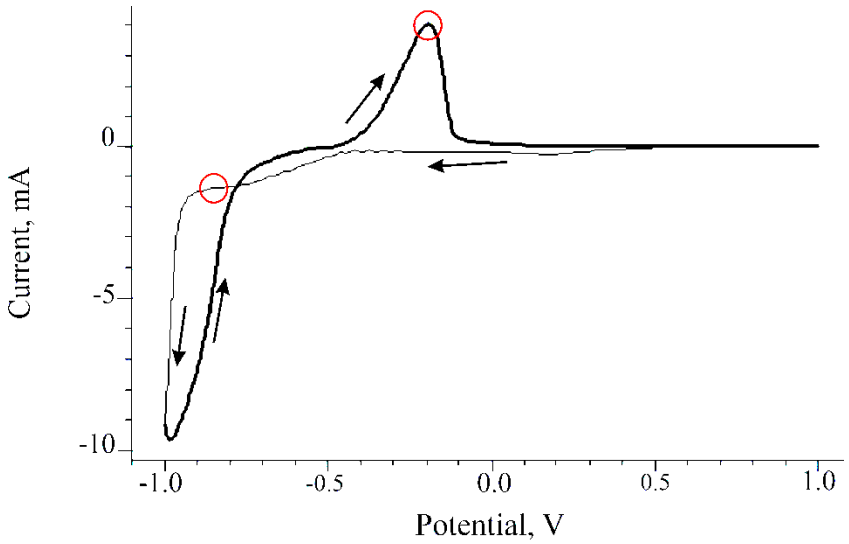

Figure 1. *Cyclic polarization curve for the co-deposition of cobalt with phosphorus. Electrolyte composition: 0.1 M $CoSO_4$; 0.12 M NaH_2PO_4; 0.5 M H_3BO_3; 0.14 M Na_2SO_4; 0.001 M $NaC_{12}H_{25}SO_4$, pH 3.6, T = 50 °C, scan rate v = 0.02 V s^{-1}*

The reduced atoms are adsorbed on the surfaces of nanoparticles, where phosphorus atoms diffuse and incorporate into the cobalt crystal lattices, forming the Co-P phase [32,33]. X-ray phase analysis of the annealed Co-P thin film, carried out in air, revealed two cobalt compounds: Co_2P and CoP (Figure 2).

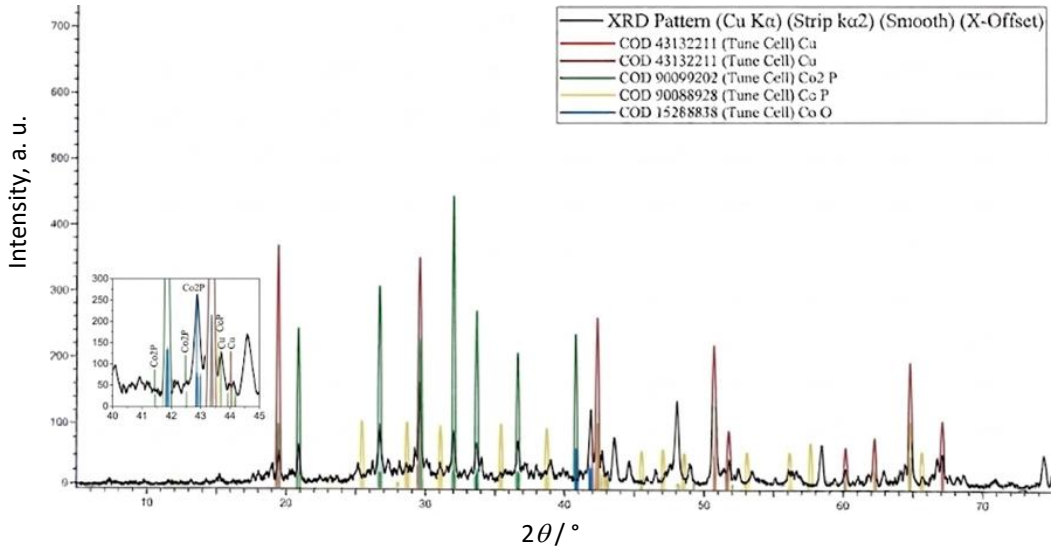

Figure 2. *X-ray diffraction pattern of deposited Co-P thin film after annealing.*

XRD Pattern (Cu Kα) (Strip Kα$_2$) (Smooth) (X-Offset): *Experimental X-ray diffraction pattern collected using Cu Kα radiation. Strip Kα$_2$ indicates that the Cu Kα$_2$ component was removed from the diffraction data during processing. Smooth indicates that a smoothing algorithm was applied to reduce statistical noise without altering the diffraction peaks. X-Offset denotes a horizontal shift applied only for graphical presentation to improve the visualization of overlapping patterns; it does not affect the diffraction angles or phase identification.*

COD 43132211 (Tune Cell) Cu: *Reference diffraction pattern of Cu from the Crystallography Open Database (COD). Tune Cell indicates that the unit-cell parameters of the reference structure were optimized by the software to improve alignment with the experimental diffraction pattern.*

COD 90099202 (Tune Cell) Co$_2$P: *Reference diffraction pattern of Co_2P from the COD database. Tune Cell denotes software optimization of the reference unit-cell parameters for pattern matching.*

COD 90088928 (Tune Cell) CoP: *Reference diffraction pattern of CoP from the COD database. Tune Cell indicates optimization of the reference unit-cell parameters during phase matching.*

COD 15268838 (Tune Cell) CoO: *Reference diffraction pattern of CoO from the COD database. Tune Cell indicates software refinement of the reference unit-cell parameters for comparison with the experimental pattern*

Co-P system coatings produced by electrochemical deposition are frequently formed in an amorphous or amorphous-nanocrystalline state. After heat treatment, crystallization and phase segregation typically occur, leading to the formation of cobalt phosphide phases. In the present study, two orthorhombic phases, Co_2P and CoP, were identified after annealing [34].

The formation of cobalt phosphides proceeds according to Equations (4) and (5) [31,35]:

$$Co + P \rightarrow CoP \quad (4)$$

At the initial stage, the co-electrodeposition proceeds according to Equation (4); subsequently, with an increased cobalt content in the deposited film, Co_2P is formed according to Equation (5):

$$2Co + P \rightarrow Co_2P \quad (5)$$

The presence of CoO in the X-ray diffraction pattern is attributed to the annealing of the obtained film in air, while the presence of copper originates from the substrate material on which the film was deposited. The film consists of two phases: the CoP phase and the cobalt-rich Co_2P phase.

Figure 3 presents linear polarization curves for the co-deposition of cobalt and phosphorus at different scan rates (Figure 3a) and the dependence of the peak current density on the square root of the scan rate (Figure 3b).

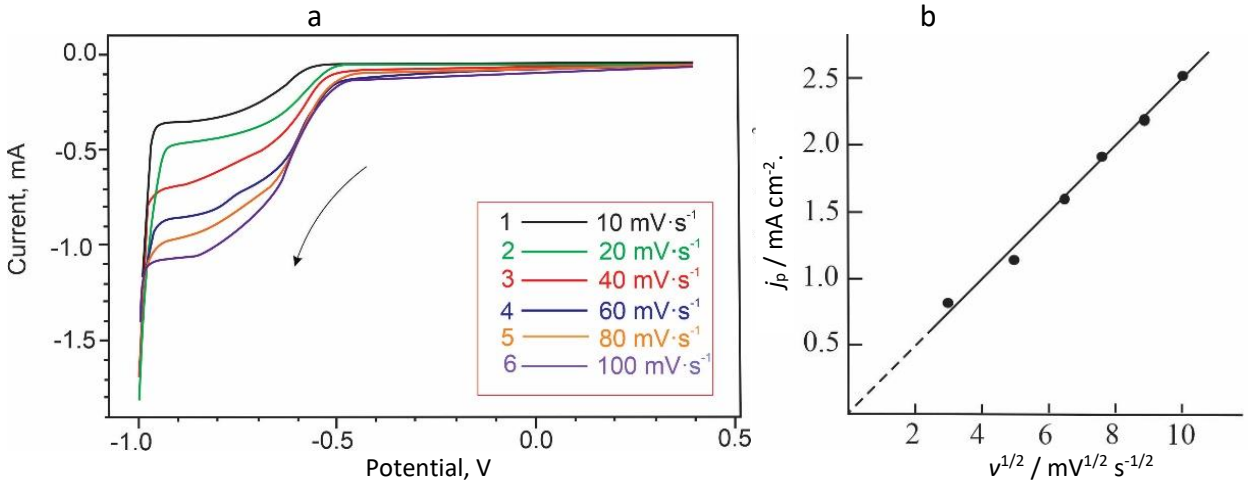

Figure 3. *a) Linear polarization curves for the co-deposition of cobalt with phosphorus at different potential scan rates, electrolyte composition: 0.1 M $CoSO_4$; 0.12 M NaH_2PO_4; 0.5 M H_3BO_3; 0.14 M Na_2SO_4; 0.001 M $NaC_{12}H_{25}SO_4$, pH 3.6, T = 50 °C, b) dependence of peak current density on the square root of sweep rate*

The scan rate has no significant effect on the co-deposition process. Only the co-deposition potential shifts slightly toward more positive values as the scan rate increases. Based on these curves, the dependence of j_p *vs.* $v^{1/2}$ (Figure 3b) was constructed. This relationship is linear, which, according to the Randles-Ševčík equation, is characteristic of processes in which the rate-determining step is the diffusion of the depositing ions [36].

Chronoamperometric and chronopotentiometric studies of the co-deposition of cobalt with phosphorus were also carried out. Figure 4a presents the chronoamperometric curves for the co-deposition of Co with P at various deposition potentials. The figure clearly shows that the current intensities in all six curves initially rise sharply and then stabilize. Stabilization occurs approximately 1.2 to 1.4 seconds after the onset of deposition. The rapid increase in current to its maximum is due to the charging of the electrical double layer on the electrode surface. As a result, Co ions are rapidly reduced, and the cobalt content on the electrode surface increases with deposition time.

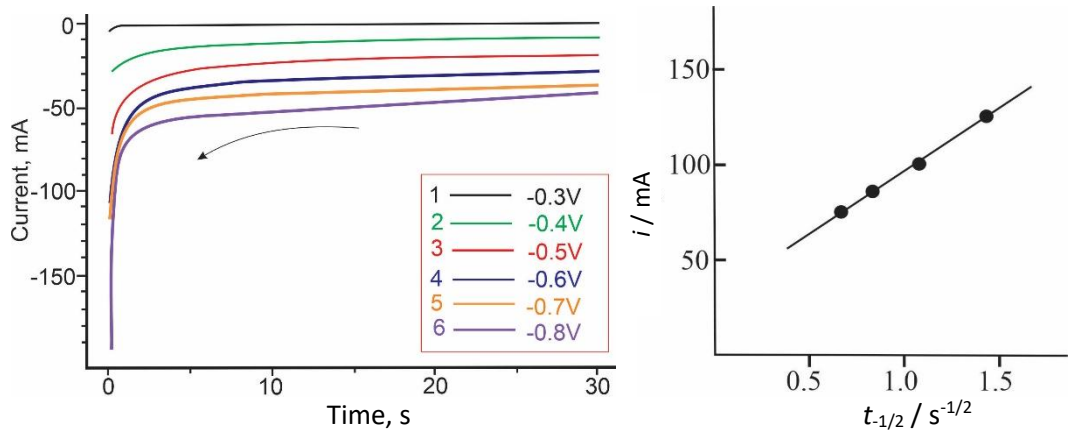

Figure 4. *(a) Chronoamperometric curves for the co-deposition of cobalt with phosphorus at different deposition potentials (-0.3 to -0.8 V) from an electrolyte with composition: 0.1 M $CoSO_4$; 0.12 M NaH_2PO_4; 0.5 M H_3BO_3; 0.14 M Na_2SO_4; 0.001 M $NaC_{12}H_{25}SO_4$, pH 3.6,* T *= 50 °C, (b) dependence of the* i vs.$t^{-1/2}$ *at -0.8 V*

According to the Scharifker-Hills model [37], two types of nucleation processes exist: instantaneous and progressive. Instantaneous nucleation implies the simultaneous growth of nuclei upon application of the deposition potential, whereas in progressive nucleation, nuclei form continuously during electrodeposition. Equation (6) describes the theoretical transient model for instantaneous nucleation, while Equation (7) describes progressive three-dimensional nucleation:

$$\left(\frac{i(t)}{i_{max}}\right)^2 = \frac{1.9542}{t/t_{max}}\left(1\text{-}e^{-1.2564\, t/t_{max}}\right)^2 \quad (6)$$

$$\left(\frac{i(t)}{i_{max}}\right)^2 = \frac{1.2254}{t/t_{max}}\left(1\text{-}e^{-2.3367\left(t/t_{max}\right)^2}\right)^2 \quad (7)$$

where t_{max} / s is the time at the maximum current i_{max} / A.

At the onset of deposition, at potentials up to -0.3 V, the chronoamperometric curve for the co-deposition follows the instantaneous nucleation model, in which Co-P nuclei form simultaneously at multiple active sites on the substrate surface. At higher potentials (from -0.4 to -0.8 V), deposition occurs according to the progressive nucleation model. The electrochemical behaviour of the depositing ions can be further analysed based on the relationship between $I(t)$ and $t^{-1/2}$. This relationship is shown in Figure 4b, constructed from the data in Figure 4a. Figure 4b demonstrates that $i(t)$ exhibits a strong linear correlation with $t^{-1/2}$, indicating that the co-deposition of cobalt with phosphorus is controlled by the diffusion of ions to the electrode surface.

The diffusion coefficient was calculated using the Sand Equation (8) [38] for four different deposition potentials according to the following formula:

$$\tau = \frac{n^2F^2\pi DC_b^{\,2}}{4j^2} \quad (8)$$

where τ / s is transition time, n is the number of electrons participating in the reaction, F is the Faraday constant (96485 C mol^{-1}), D / cm^2 s^{-1} is diffusion coefficient of the electroactive substance, C_b / mol cm^{-3} is volume concentration of the substance in the solution and j / A cm^{-2} is current density.

The nucleus (or nucleation) density was calculated using the Scharifker method [37].

Table 1 presents the diffusion coefficient and the nucleation density (N_o) at four different deposition potentials. The table shows that increasing the cathode potential accelerates the electrochemical reaction and reduces the concentration of deposited ions in the near-electrode layer. As a result, mass transfer becomes more difficult, the thickness of the diffusion layer

increases, and the effective diffusion coefficient calculated from electrochemical data may decrease, although this is not directly consistent with the Randles-Ševčik equation. The table also shows that the nucleation density N_0 increases sharply with increasing deposition potential. This behaviour can be attributed to the enhanced activity of nucleation sites at higher deposition potentials. This behaviour can be explained by the increased activity of nucleation sites at higher deposition potentials. The average diffusion coefficient for the deposition process was determined to be 1.8×10^{-5} cm² s^{-1}.

Table 1. *The experimental data of the CA deposition of Co-P*

Applied potential, V	D / 10^{-5} cm^2 s^{-1}	N_0 / 10^{18} cm^{-3}
-0.3	2.07	12.3
-0.5	1.75	25.72
-0.6	1.53	37.64
-0.8	1.22	48.14

Figure 5 shows the chronopotentiometric studies of the co-deposition of cobalt with phosphorus. The curves indicate that the electrode potential initially decreases (from 0.3 s to 5 s) and then stabilizes after approximately 10 seconds.

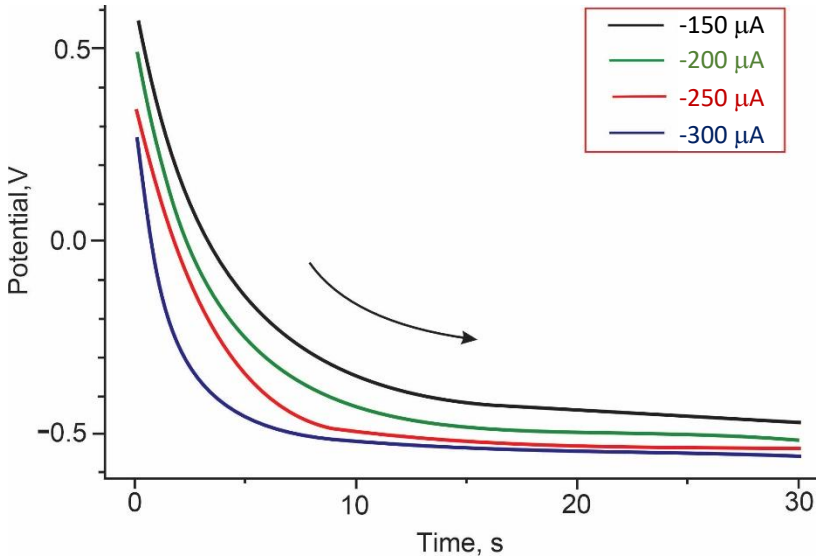

Figure 5. *Chronopotentiometric curves at different current intensities for the co-deposition of Co with P (electrolyte composition as in Figure 4)*

The ohmic polarization of the electrolyte, arising from a constant current applied to the cathode surface, significantly alters the system's electrode potential, causing the cathode potential to decrease rapidly. This sharp potential drop is attributed to instantaneous nucleation during co-deposition. The stabilization of the potential after approximately 10 seconds of deposition can be explained by the fact that the number of depositing species at the active nucleation sites does not match the rate of cobalt nucleus formation, and the deposition process becomes controlled by concentration polarization [38]. These factors gradually reduce the current until a steady state is reached. After this stage, no new nuclei are formed; only the growth of existing nuclei occurs on the cathode surface. This contributes to an increase in the real surface area of the electrode and its passivation. This behaviour of the chronopotentiometric polarization curve can also be explained by the simultaneous evolution of hydrogen on the cathode surface during alloy deposition.

The chronopotentiometric curve of the electrodeposition process from the investigated bath demonstrates an initial short phase of higher overpotential due to the nucleation of Co and P

particles on the substrate surface, followed by a phase of relatively constant potential corresponding to the growth of Co-P particles after nucleation. Three distinct regions can be identified on the potential curve recorded during electrodeposition: a short region of high potential, a broad potential peak, and a gradual decrease in potential. The region of elevated potential can be attributed to the depletion of Co and P ions near the electrode surface. The subsequent broad peak reflects strong inhibition at the early stage of Co-P deposit growth, due to the adsorption of these ions on the metal substrate surface, driven by Coulombic attraction between the depositing ions and the electrode. This adsorption leads to the formation of micelle-like structures or hydrophobic double layers on the electrode surface. At the final stage of deposition, the potential gradually increases, which can be attributed to the expansion of the electrode's electroactive surface area.

When recording polarization curves, an inert material is typically used to avoid side reactions on the electrode surface that could interfere with the study of the co-deposition mechanism.

Figure 6 presents the results of the morphological analysis of the Co-P thin film on a copper substrate obtained using SEM. The growth of Co-P nanostructures was observed at potentials of -0.5 to -0.7 V. At these potential values, clusters of Co-P nanospheres are formed, resembling a cauliflower-like structure, with an average particle size of 15.6 to 18.0 μm (Figure 6a).

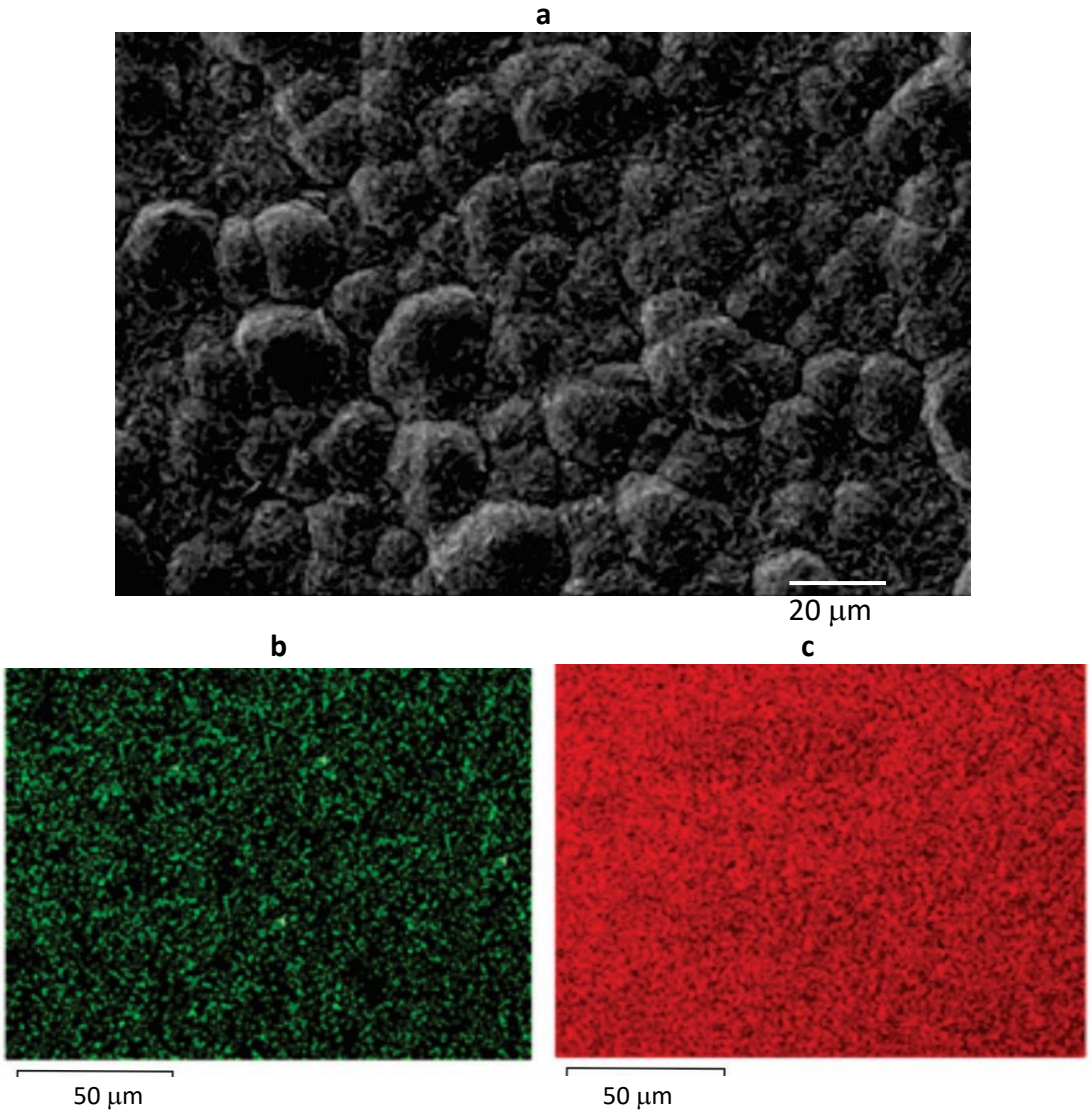

Figure 6. *SEM analysis results of the Co-P thin film deposited on copper plate: (a) Co-P coating; (b) Co; (c) P*

Figure 7 shows the cross-section of the Co-P alloy with marked points used to determine the composition of the film along its depth.

The depth analysis of the film showed that the topmost layer consists mainly of cobalt oxide. Phosphorus appears already at the second point, and its concentration increases from 1.49 wt.% to 45.32 wt.% at point 5. Then, the phosphorus content decreases to 0.27 wt.% at point 7. From this image, the film thickness was determined to be 176.364 μm.

The overall composition profile of the investigated Co-P film, determined by the EDX method, is shown in Figure 8. It can be seen from the figure that the average phosphorus content is up to 6.7 %.

The results of SEM and EDX analyses confirmed the X-ray diffraction data of the obtained thin film, which consisted of Co, P and O_2.

Considering that according to literature data, Co-P alloys exhibit bifunctional catalytic behaviour, the electrocatalytic properties of the obtained alloy were investigated for both HER and OER in neutral and alkaline media.

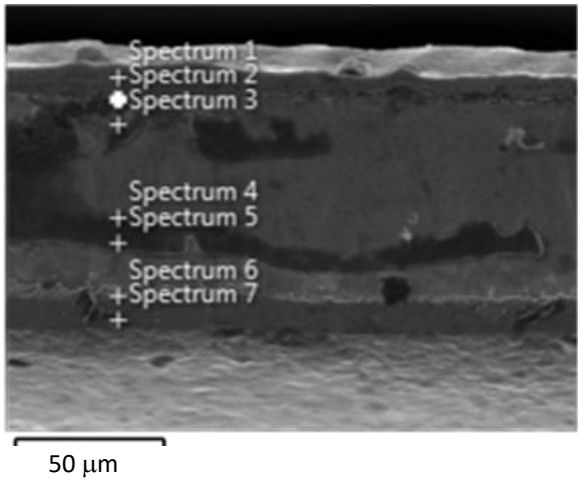

Figure 7. *Cross-section of the Co-P thin film deposited on copper plate. Spectrum 1 to 7 indicate the EDS analysis locations and the + symbols mark the corresponding analysis points*

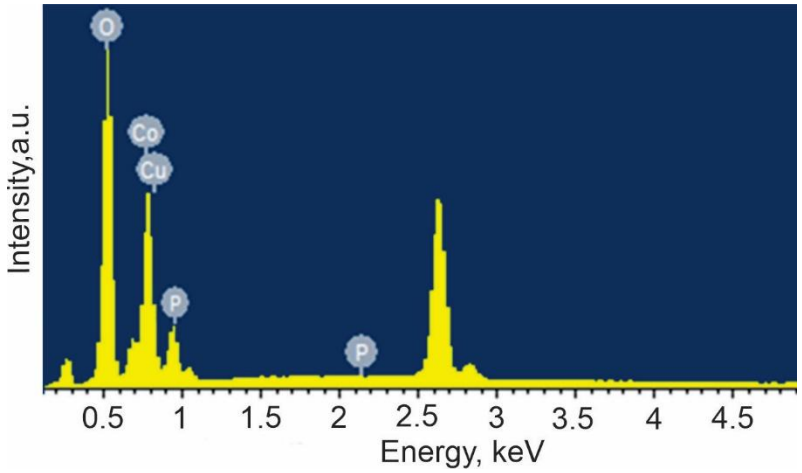

	Content, at.%
P	6.7
Co	62.69
Cu	9.40
O	21.21

Figure 8. *EDS analysis results of the Co-P thin film deposited on copper plate*

Figure 9 shows the cathodic polarization curves of the Co-P thin film in neutral (Figure 9a) and alkaline (Figure 9b) media for HER, both before and after annealing (heat treatment). The obtained film served as the cathode, while a platinum plate was used as the anode.

It can be seen from Figure 9 that in both neutral and alkaline environments, the electrocatalytic activity of the amorphous film is higher than that of the film subjected to annealing.

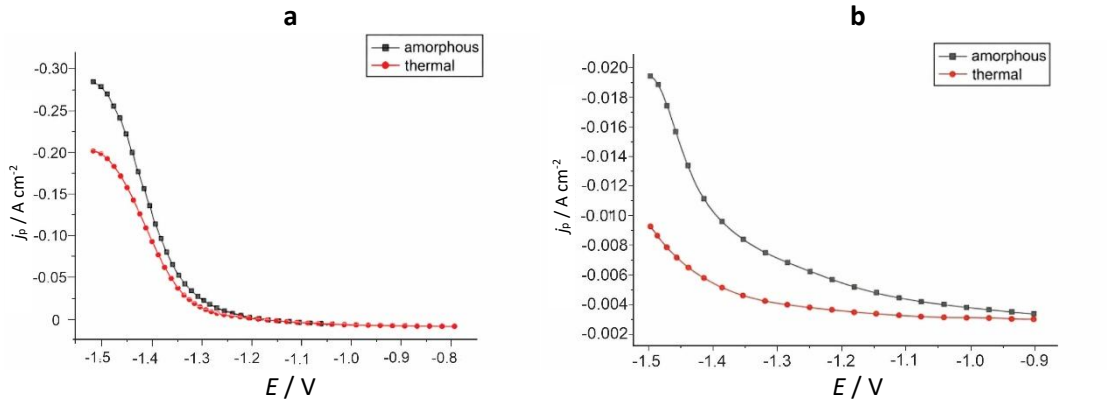

Figure 9. *Polarization curves demonstrating electrocatalytic activity of as-deposited (amorphous) and annealed (thermal) Co-P electrocatalysts toward HER: (a) in a neutral medium (0.5 M Na_2SO_4); (b) in an alkaline medium (1 M KOH)*

LSV (linear sweep voltammetry) and Tafel plots were constructed based on these polarization curves for studies in neutral (Figure 10) and alkaline (Figure 11) media, and the corresponding Tafel slope values were determined.

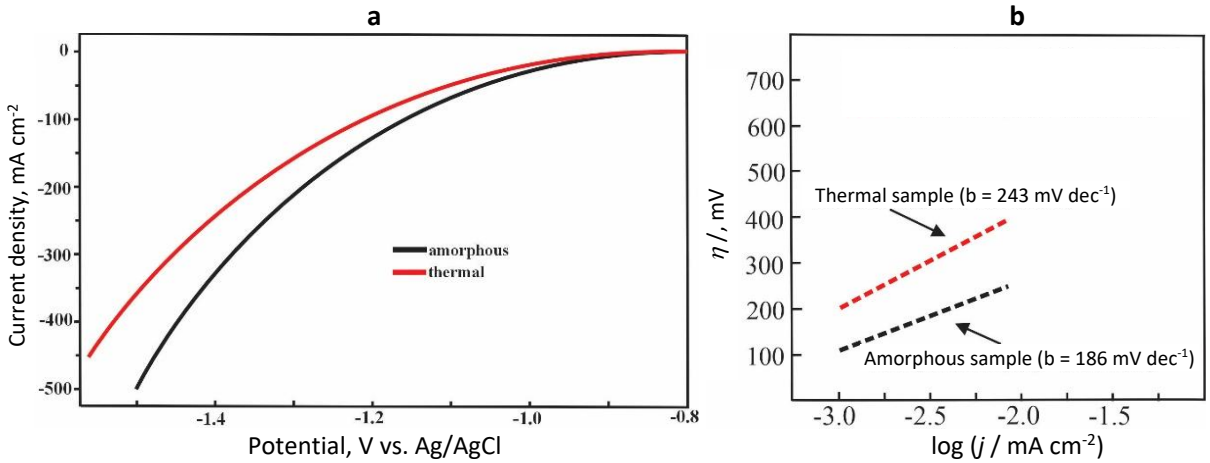

Figure 10. *(a) Linear sweep voltammetry of as-deposited (amorphous) and annealed (thermal) Co-P electrocatalysts for the HER in 0.5 M Na_2SO_4, at 298K (b) Tafel plots of hydrogen evolution reaction*

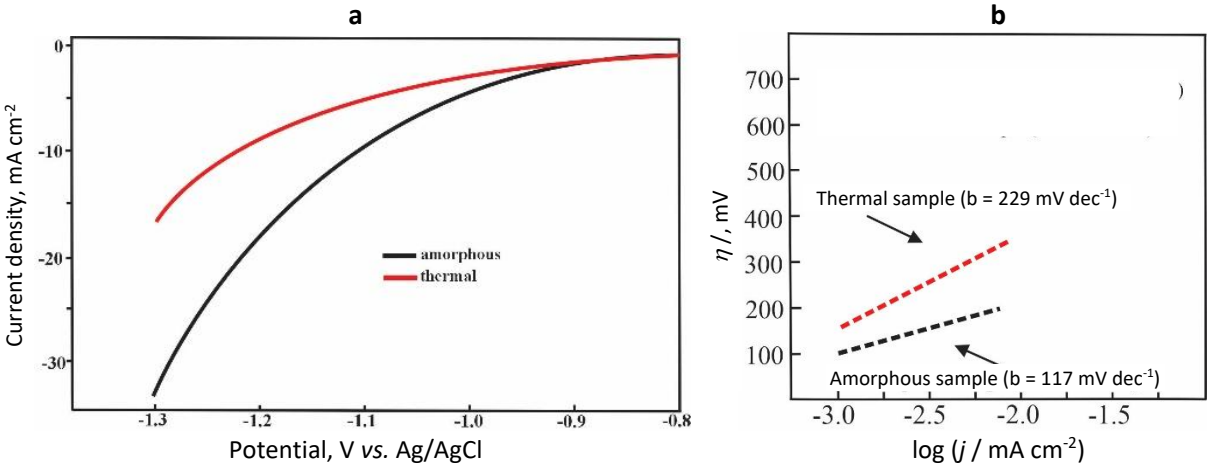

Figure 11. *(a) Linear sweep voltammetry of as-deposited (amorphous) and annealed (thermal) Co-P for the hydrogen evolution reaction in 1 M KOH, at 298 K, (b) Tafel plots of hydrogen evolution reaction*

It was found that the electrocatalytic activity of the as-deposited (amorphous) Co-P thin film was higher, exhibiting a Tafel slope value of 186 mV dec^{-1} compared to the annealed film, which showed

a Tafel slope of 243 mV dec^{-1}. The overpotential (η) for the amorphous film in a neutral environment was 142 mV, in an alkaline environment 48 mV, and for the annealed film, the overpotential in a neutral environment was 152 mV, in an alkaline environment 61.8 mV at a current density of 10 mA cm^{-2}.

In an alkaline medium, the electrocatalytic activity toward HER of the as-deposited (amorphous) Co-P thin film, with a Tafel slope value of 117 mV dec^{-1}, was higher than that of the annealed film, which exhibited a Tafel slope value of 229 mV dec^{-1}.

To evaluate the electrocatalytic activity of the obtained Co-P film for the OER, polarization curves were recorded in both neutral and alkaline media, where the prepared film served as the anode (Figure 12). In neutral medium, higher OER activity is observed for the amorphous Co-P film, while in alkaline medium, for the thermal (annealed) film.

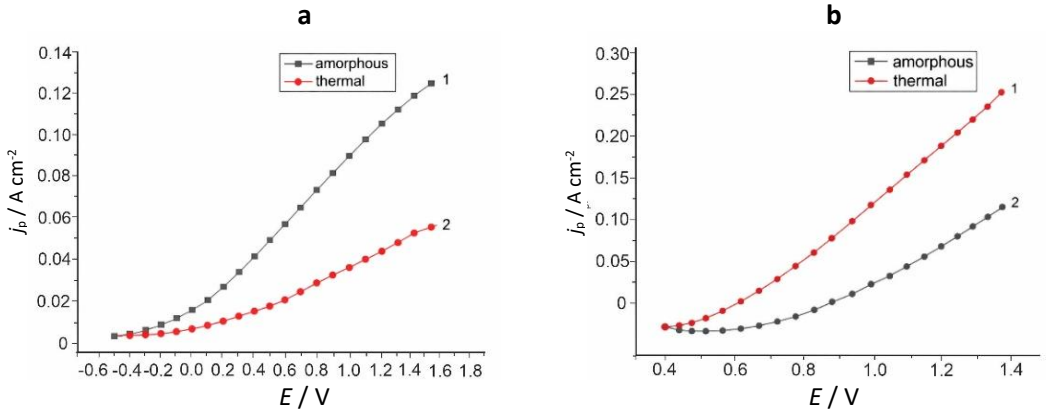

Figure 12. *Electrocatalytic activity of as-deposited (amorphous) and annealed (thermal) Co-P thin film electrocatalysts toward OER: (a) in a neutral medium (0.5 M Na_2SO_4), (b) in an alkaline medium (1 M KOH)*

In Figure 13, LSV and Tafel plots for the OER were constructed from the data in Figure 12 for both neutral (Figure 13) and alkaline (Figure 14) media. In a neutral medium, the electrocatalytic activity of the annealed films in the OER was lower (Figure 13a), exhibiting a Tafel slope value of 138 mV dec^{-1}, compared to the non-annealed electrodes, which showed a Tafel slope value of 77 mV dec^{-1} (Figure 13b).

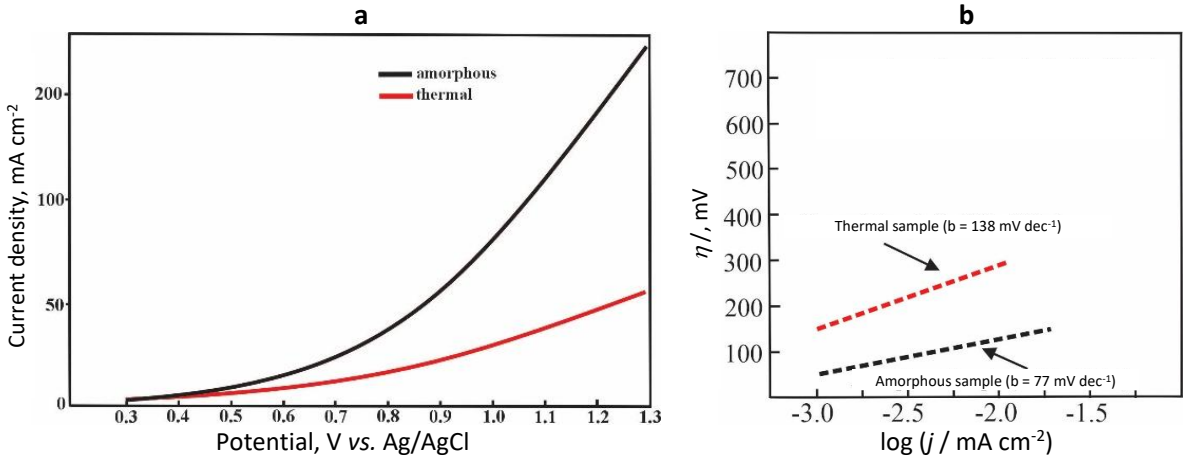

Figure 13. *(a) Linear sweep voltammetry of as-deposited (amorphous) and annealed (thermal) Co-P electrocatalysts for the OER in 0.5 M Na_2SO_4, at 25 °C, (b) Tafel plots of oxygen evolution reaction*

Tests conducted with the same electrodes in an alkaline medium for OER showed that the annealed Co-P films, with a Tafel slope value of 119 mV dec^{-1}, exhibited higher activity than the amorphous (non-annealed) films, which had a Tafel slope value of 235 mV dec^{-1}.

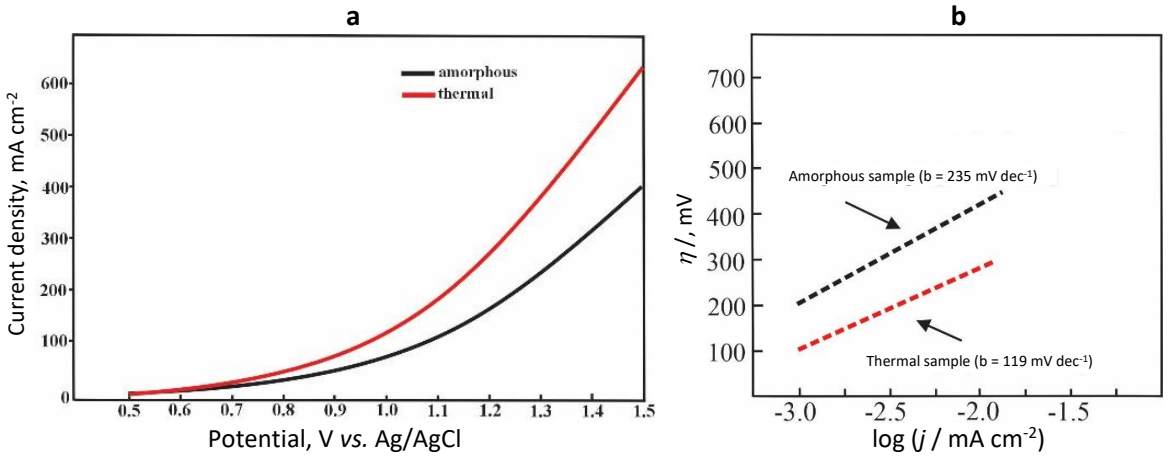

Figure 14. *(a) Linear sweep voltammetry of the Co-P electrocatalyst for the OER in 1M KOH, (b) Tafel plots of oxygen evolution reaction on the deposited electrocatalytic materials in 1 M KOH at 298 K*

Table 2 presents comparative values of the Tafel slope and overpotential at a current density of 10 mA cm^{-2} for Co-P reported by other authors.

Table 2. *Comparison of the catalytic performance of Co-P in HER and OER with previously published studies in alkaline and neutral media*

References	Tafel slope, mV dec^{-1}				η / mV (at 10 mA cm^{-2})			
	In neutral medium		In alkaline medium		In neutral medium		In alkaline medium	
	HER	OER	HER	OER	HER	OER	HER	OER
[39]	-	-	34.1	61.7	-	-	107.6	400
[40]	-	-	124.5	99.0	-	-	207.0	340
[41]	-	-	147.0	80.0	-	-	69.0	326
[42]	-	-	124.5	69.5	-	-	207.0	361
our work	186	77	117.0	190	142	50	48.0	171

The lowest Tafel slope for the HER in alkaline media was reported for Co-P films, with a value of 34.1 mV dec ^{1}; however, the overpotential at 10 mA cm^{-2} was 107.6 mV [40]. In our work, the Tafel slope value in alkaline medium was 117 mV dec^{-1} with an overpotential of 48 mV, *i.e.* almost two times lower. For the OER in the same study, the Tafel slope value was 61.7 mV dec^{-1} at η = 400 mV. The overpotential for the OER on our electrode is 2.33 times lower. This indicates the superior electrocatalytic activity of the electrode in both reactions during water electrolysis.

An important requirement for electrocatalysts used in HER and OER is high corrosion resistance in the working medium. Since alkaline electrolytes are commonly employed in industrial hydrogen production, the corrosion properties of the obtained films were investigated in an alkaline environment.

To evaluate the operational stability of the synthesized Co-P thin films, chronopotentiometric measurements were performed in a 1 M KOH solution during the HER at 25 °C and a current density of 10 mA cm^{-2}. Figure 15 shows the dependence of potential on time for the annealed sample (red line) and the as-deposited sample (black line) during HER (Figure 15a) over 12 and 10 hours of electrolysis, respectively, and during OER (Figure 15b) over 11.5 and 9 hours of electrolysis, respectively. The curves exhibit linear behaviour, with lines parallel to the abscissa, indicating high operational stability of the obtained Co-P thin films in alkaline media over the investigated time periods [43].

Corrosion properties were evaluated by recording cathodic and anodic polarization curves, after which the corrosion rate of the Co-P alloys was determined for both HER and OER. The data obtained by Tafel extrapolation and automatically calculated using Gamry Instruments for HER are as follows: the corrosion resistance of the amorphous Co-P film was 626.9 Ω, the corrosion rate was 16.11 μm year^{-1}, and the corrosion current density (j_{corr}) was 1.387 μA cm^{-2}.

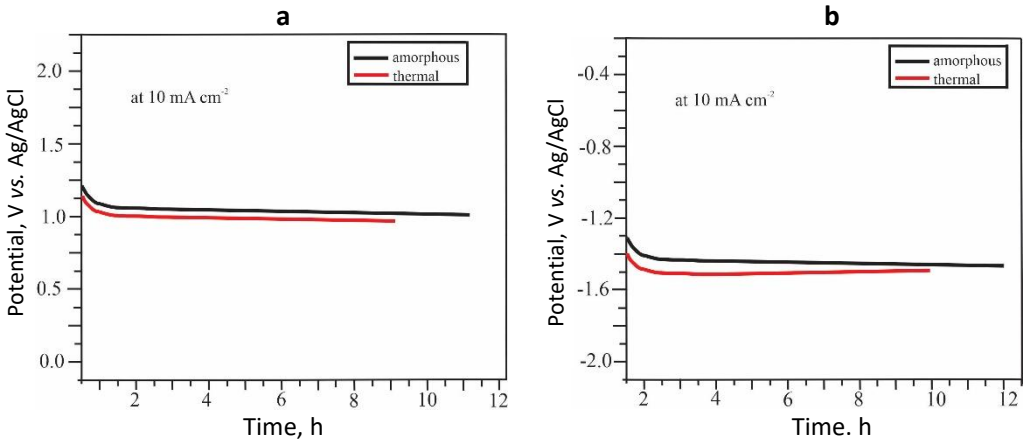

Figure 15. *Chronopotentiometric curves of the as-deposited (amorphous) and annealed (thermal) Co-P thin films in 1 M KOH over 12 hours: (a) HER; (b) OER*

For OER, the corrosion resistance was 210.5 Ω, the corrosion rate was 1.351 mm year^{-1}, and the corrosion current density (j_{corr}) was 116.3 μA cm^{-2}. These values were calculated for a geometric surface area of 1 cm^2. However, we calculated these values for a geometric area of 2 cm^2 without using the instrument.

EDX analysis showed a deposit density of 7.36 g cm^{-3}, which differs from the instrument-reported value of 7.86 g cm^{-3}, and the corrosion rate (CR, mm year^{-1}) was calculated using Equation (9):

$$CR = \frac{Kj_{corr}M}{n\rho} \quad (9)$$

where j_{corr} / A cm^{-2} is the corrosion current density, M / g mol^{-1} is the molar mass of the metal, n is the number of electrons involved in the reaction, ρ / g cm^{-3}is the density, and K is a constant (for μm year^{-1}, typically 3.27).

After calculation using Equation (9), the obtained CR values were 8.8 μm year^{-1}, while polarization resistance was 1253.8 Ω cm^2, and corrosion current density (j_{corr}) of 0.6859 μA cm^{-2}.

The results indicate that the corrosion resistance of amorphous Co-P thin films is higher than that of annealed samples. This is because amorphous alloys more readily form dense, uniform, and passive deposits, whereas crystalline materials contain grain boundaries, which are energetically unstable regions. This promotes the accelerated diffusion of aggressive ions in the medium (OH^- and SO_4^{2-}), thereby facilitating the corrosion of the deposited films [44].

Conclusions

In conclusion, the co-deposition of cobalt with phosphorus is initially controlled by a diffusion-limited stage and subsequently governed by mixed kinetics. At the early stage of the process, crystal nucleation proceeds *via* an instantaneous nucleation mechanism, followed by progressive nucleation. The Co-P thin films obtained under the proposed conditions exhibit bifunctional catalytic activity and are suitable for hydrogen production *via* water electrolysis in both neutral and alkaline media. During alkaline water electrolysis, the as-deposited amorphous Co-P thin film effectively serves as the cathode, while the annealed film functions as the anode. Corrosion resistance studies demonstrated that amorphous Co-P films exhibit greater corrosion stability than annealed samples in both the hydrogen and oxygen evolution reactions under alkaline conditions.

Funding: *This study was funded by the Ministry of Science and Higher Education of Azerbaijan.*

References

[1] D. Larcher, J. M. Tarascon, Towards greener and more sustainable batteries for electrical energy storage, *Nature Chemistry* **7(1)** (2015) 19-29. https://doi.org/10.1038/NCHEM.2085

[2] D. E. Grineva, R. M. Mensharapov, N. A. Ivanova, D. D. Spasov, M. V. Sinyakov, A. Sh. Aliyev, V. N. Fateev, Hydrogen-supported decarbonization of automotive industry: from ICE through hybrids to FC vehicles, *International Journal of Hydrogen Energy* **192** (2025) 152238. https://doi.org/10.1016/j.ijhydene.2025.152238

[3] G. Tatishvili, A. Aliyev, N. Bolashvili, M. Tsatsanashvili, N. Nioradze, L. Kvinikadze, Green hydrogen energy prospects: Georgia-Azerbaijan strategic partnership, *International Journal of Hydrogen Energy* **193** (2025) 152258. https://doi.org/10.1016/j.ijhydene.2025.152258

[4] Y. Liu, Y. Zhang, Z. Sun, L. Dai, B. Liu, W. Li, Catalysts with three-dimensional porous structure for electrocatalytic water splitting, *Sustainable Materials and Technologies* **44** (2025) e01392. https://doi.org/10.1016/j.susmat.2025.e01392

[5] A. Sh. Aliyev, R. G. Guseynova, U. M. Gurbanova, D. M. Babanly, V. N. Fateev, I. V. Pushkareva, D. B. Tagiyev, Electrocatalysts for water electrolysis, *Chemical Problems* **16(3)** (2018) 283-306. https://doi.org/10.32737/2221-8688-2018-3-283-306

[6] A. Sh. Aliyev, R. G. Huseynova, U. M. Gurbanova, A. O. Zeynalova, D. B. Tagiyev, Green hydrogen is the energy source of the future, *Azerbaijan Chemical Journal* **2** (2025) 5-20. https://doi.org/10.32737/0005-2531-2025-2-5-20

[7] J. Wu, N. Liu, F. Li, B. Jia, J. Zheng, Iron group elements (Fe, Co, Ni) in Electrocatalytic applications: Evaluation, characterization and prospects, *Coordination Chemistry Reviews* **525** (2025) 216343. https://doi.org/10.1016/j.ccr.2024.216343

[8] U. M. Gurbanova, D.M.Babanly, R. G. Huseynova, D. B. Tagiyev, Study of electrochemical deposition of Ni-Mo thin films from alkaline electrolytes, *Journal of Electrochemical Science and Engineering* **11(1)** (2021) 39-49. https://doi.org/10.5599/jese.912

[9] X. Chen, M. Cheng, D. Chen, R. Wang, Shape-controlled synthesis of Co_2P nanostructures and their application in supercapacitors, *ACS Applied Materials & Interfaces* **8(6)** (2016) 3892-3900. https://doi.org/10.1021/acsami.5b10785

[10] C. An, Y. Wang, Y. Wang, G. Liu, L. Li, F. Qiu, Y. Xu, L. Jiao, H. Yuan, Facile synthesis and superior supercapacitor performances of Ni_2P/rGO nanoparticles, *RSC Advances* **3(14)** (2013) 4628-4633. https://doi.org/10.1039/C3RA00079F

[11] X. Li, A. M. Elshahawy, C. Guan, J. Wang, Metal phosphides and phosphates-based electrodes for electrochemical supercapacitors, *Nano Micro Small* **13(39)** (2017) 1701530. https://doi.org/10.1002/smll.201701530

[12] A. O. Zeynalova, N. Sh. Soltanova, U. M. Gurbanova, R. G. Huseynova, A. Sh. Aliyev, D. B. Tagiyev, Electrodeposition of Ni-Co thin films from ammonia-chloride electrolyte, *Journal of Electrochemical Science and Engineering* **15(3)** (2025) 2666. https://doi.org/10.5599/jese.2666

[13] Y. Zhang, L. Li, H. Su, W. Huang, X. Dong, Binary metal oxide: advanced energy storage materials in supercapacitors, *Journal of Materials Chemistry A* **3(1)** (2015) 43-59. https://doi.org/10.1039/C4TA04996A

[14] X. Li, R. Ding, W. Shi, Q. Xu, L. Wang, H. Jiang, Z. Yang, E. Liu, Hierarchical mesoporous Ni-P@ MnO_2 composite for high performance supercapacitors, *Materials Letters* **187** (2017) 144-147. https://doi.org/10.1016/j.matlet.2016.10.021

[15] X. Wang, H. M. Kim, Y. Xiao, Y. K. Sun, Nanostructured metal phosphide-based materials for electrochemical energy storage, *Journal of Materials Chemistry A* **4(39)** (2016) 14915-14931. https://doi.org/10.1039/C6TA06705K

[16] Y. Lu, J. K. Liu, X. Y. Liu, S. Huang, T. Q. Wang, X. L. Wang, S. X. Mao, Facile synthesis of Ni-coated Ni_2P for supercapacitor applications, *CrystEngComm* **15(35)** (2013) 7071-7079. https://doi.org/10.1039/C3CE41214H

[17] Z. Pu, Q. Liu, P. Jiang, A. M. Asiri, A. Y. Obaid, X. Sun, CoP nanosheet arrays supported on a Ti plate: an efficient cathode for electrochemical hydrogen evolution, *Chemistry of Materials* **26(15)** (2014) 4326-4329. https://doi.org/10.1021/cm501273s
[18] Z. Huang, Z. Chen, Z. Chen, C.Lv, M. G.Humphrey, C.Zhang, Cobalt phosphide nanorods as an efficient electrocatalyst for the hydrogen evolution reaction, *Nano Energy* **9** (2014) 373-382. https://doi.org/10.1016/j.nanoen.2014.08.013
[19] Q. Liu, J. Tian, W. Cui, P. Jiang, N. Cheng, A. M.Asiri, X. Sun, Carbon nanotubes decorated with CoP nanocrystals: a highly active non-noble-metal nanohybrid electrocatalyst for hydrogen evolution, *Angewandte Chemie International Edition* **53(26)** (2014) 6710-6714. https://doi.org/10.1002/anie.201404161
[20] Y. Wang, Y. Wang, H. Li, Z. Liu, L. Zhang, H. Jiang, N. Ren, Facile synthesis of Co_2P via the reduction of phosphate with KBH4 for nickel-based rechargeable batteries, *Journal of Alloys and Compounds* **623** (2015) 140-145. https://doi.org/10.1016/j.jallcom.2014.10.100
[21] J. F. Callejas, J. M. McEnaney, C. G. Read, J. C. Crompton, A. J. Biacchi, E. J. Popczun, R. E. Schaak, Electrocatalytic and photocatalytic hydrogen production from acidic and neutral-pH aqueous solutions using iron phosphide nanoparticles, *ACS Nano* **8(11)** (2014) 11101-11107. https://doi.org/10.1021/nn5048553
[22] J. F. Callejas, C. G. Read, C. W. Roske, N. S. Lewis, R. E. Schaak, Synthesis, characterization, and properties of metal phosphide catalysts for the hydrogen-evolution reaction, *Chemistry of Materials* **28(17)** (2016) 6017-6044. https://doi.org/10.1021/acs.chemmater.6b02148
[23] J. Nan, Y. Bo, S. Meili, S. Yujie, Electrodeposited Cobalt-Phosphorous-Derived Films as Competent Bifunctional Catalysts for Overall Water Splitting, *Angewandte Chemie International Edition* **54(21)** (2015) 6251-6254. https://doi.org/10.1002/anie.201501616
[24] A. Dutta, N. Pradhan, Developments of metal phosphides as efficient OER precatalysts. *The Journal of Physical Chemistry Letters* **8(1)** (2017) 144-152. https://doi.org/10.1021/acs.jpclett.6b02249
[25] A. Dong, T. Yang, J. Xue, H. Gao, L. Che, Transition metal phosphide electrocatalysts for efficient oxygen evolution reaction, *Applied Surface Science* **708** (2025) 163769. https://doi.org/10.1016/j.apsusc.2025.163769
[26] H. Zhao, Z. Y. Yuan, Engineering of transition metal phosphide-based heterostructures for electrocatalytic water splitting, *Smart Materials and Devices* **1(3)** (2025) 202521-202521. https://doi.org/10.70401/smd.2025.0013
[27] J. Huang, Y. Xiong, Z. Peng, L. Chen, L. Wang, Y. Xu, Y. Chen, A general electrodeposition strategy for fabricating ultrathin nickel cobalt phosphate nanosheets with ultrahigh capacity and rate performance, *ACS Nano* **14(10)** (2020) 14201-14211. https://doi.org/10.1021/acsnano.0c07326
[28] Z. Li, H. Feng, M. Song, C. He, W. Zhuang, L. Tian, Advances in CoP electrocatalysts for water splitting, *Materials Today Energy* **20** (2021) 100698. https://doi.org/10.1016/j.mtener.2021.100698
[29] J. Kim, Y. J. Jang, Y. H. Jang, Electrodeposition of stable noble-metal-free Co-P electrocatalysts for hydrogen evolution reaction, *Materials* **16(2)** (2023) 593. https://doi.org/10.3390/ma16020593
[30] G. Q. Han, X. Li, Y. R. Liu, B. Dong, W. H. Hu, X. Shang, C. G. Liu, Controllable synthesis of three dimensional electrodeposited Co-P nanosphere arrays as efficient electrocatalysts for overall water splitting, *RSC Advances* **6(58)** (2016) 52761-52771. https://doi.org/10.1039/C6RA04478F
[31] M. C. López, G. F. Ortiz, J. L. Tirado, A functionalized Co_2P negative electrode for batteries demanding high Li-potential reaction, *Journal of The Electrochemical Society* **159(8)** (2012) A1253-A1261, https://doi.org/10.1149/2.052208jes
[32] F. H. Saadi, A. I. Carim, E. Verlage, J. C. Hemminger, N. S. Lewis, M. P. Soriaga, CoP as an acid-stable active electrocatalyst for the hydrogen-evolution reaction: electrochemical synthesis,

interfacial characterization and performance evaluation, *The Journal of Physical Chemistry C* **118(50)** (2014) 29294-29300. https://doi.org/10.1021/jp5054452

[33] D. H. Ha, L. M. Moreau, C. R. Bealing, H. Zhang, R. G. Hennig, R. D. Robinson, The structural evolution and diffusion during the chemical transformation from cobalt to cobalt phosphide nanoparticles, *Journal of Materials Chemistry* **21(31)** (2011) 11498-11510. https://doi.org/10.1039/C1JM10337G

[34] M. A. Sheikholeslam, M. H. Enayati, K. Raeissi, Characterization of nanocrystalline and amorphous cobalt-phosphorous electrodeposits, *Materials Letters* **62(21-22)** (2008) 3629-3631. https://doi.org/10.1016/j.matlet.2008.04.023

[35] J. Wang, L. Zhu, G. Dharan, G. W. Ho, Electrodeposited cobalt phosphide superstructures for solar-driven thermoelectrocatalytic overall water splitting, *Journal of Materials Chemistry A* **5(32)** (2017) 16580-16584. https://doi.org/10.1039/C7TA04719C

[36] J. Elgrishi, M. B. Rountree, B. D. McCarthy, E. S. Rountree, T. T. Eisenhart, J. L. Dempsey, A Practical Beginner's Guide to Cyclic Voltammetry, *Journal of Chemical Education* **94(2)** (2017) 197-206. https://doi.org/10.1021/acs.jchemed.7b00361

[37] B. Scharifker, G. Hills, Theoretical and experimental studies of multiple nucleation, *Electrochimica Acta* **28(7)** (1983) 879-889. https://doi.org/10.1016/0013-4686(83)85163-9

[38] H. Kang, J. Li, C. Zhang, J. Lu, Q. Wang, Y. Wang, Study of the electrochemical recovery of cobalt from spent cemented carbide, *RSC Advances* **10(37)** (2020) 22036-22042. https://doi.org/10.1039/D0RA02602F

[39] H. Amber, A. Balčiūnaitė, Z. Sukackiene, L. Tamašauskaitė-Tamašiūnaitė, E. Norkus, Electrolessly Deposited Cobalt-Phosphorus Coatings for Efficient Hydrogen and Oxygen Evolution Reactions, *Catalysts* **15(1)** (2025) 8. https://doi.org/10.3390/catal15010008

[40] J. Chang, Y. Xiao, M. Xiao, J. Ge, C. Liu, X. Han, C. Zhong, W. Hu, W. Xing, Surface oxidized cobalt-phosphide nanorods as an advanced oxygen evolution catalyst in alkaline solution, *ACS Catalysis* **5(11)** (2015) 6874-6878. https://doi.org/10.1021/acscatal.5b02076

[41] M. Zhang, S. Ci, H. Li, P. Cai, H. Xu, Z. Wen, Highly defective porous CoP nanowire as electrocatalyst for full water splitting, *International Journal of Hydrogen Energy* **42** (2017) 29080-29090. https://doi.org/10.1016/j.ijhydene.2017.09.171

[42] J. Chang, L. Liang, C. Li, M. Wang, J. Ge, C. Liu, W. Xing, Ultrathin cobalt phosphide nanosheets as efficient bifunctional catalysts for a water electrolysis cell and the origin for cell performance degradation, *Green Chemistry* **18** (2016) 2287-2295. https://doi.org/10.1039/C5GC02899J

[43] M. Arnaudova, E. Lefterova, R. Rashkov, Corrosion behavior of electrodeposited nickel-based coatings with W, Mo, and TiO_x, *Journal of Solid State Electrochemistry* **28(5)** (2024) 1657-1670. https://doi.org/10.1007/s10008-023-05696-3

[44] J. Schroers, Processing of bulk metallic glass, *Advanced Materials* **22(14)** (2010) 1566-1597. https://doi:org/10.1002/adma.200902776